



**Testing Investors' Risk Expectations  
During the Covid Crisis Using the Bates  
Model**

par

Mohamad Bahij Ghrayeb

**Supervised by:** Pascal François

Sciences de la Gestion

Financial Engineering

*Mémoire présenté en vue de l'obtention du grade de  
maîtrise ès sciences en gestion*

*(M. Sc.)*

August 2022

©Mohamad Bahij Ghrayeb

# Acknowledgments

Words cannot express my gratitude to professor Pascal Francois. His ideas, advise and encouragement have been immense in helping complete this paper. I would also like to thank my parents for their continuous support and special thanks to my father. This one is for you.

# Abstract

The constant volatility across all maturities assumption is one of the main limitations of the Black-Scholes model, and one way of testing the validity of that assumption is to invert the classical formula of the Black-Scholes. We can then infer the volatility of the underlying which is consistent with the observed option price. This is what we know as implied volatility. Historical volatility is the volatility of the underlying for a given time period, whereas implied volatility is concerned with what volatility the market option price is implying today. In practice, when we plot the implied volatility across maturities, we get what is known as a smile or a skew. After the Black Monday of 1987, implied volatilities in equity markets across maturities changed in shape from smile to skew. Investors started pricing and giving more value to a steep downward event hence elevating the price (implied volatility) of the OTM options. To avoid the limitation of the constant volatility, investors began using models that assume a stochastic volatility, and we will use one of those models, the Bates model, to replicate the market options under study. The Bates model is a stochastic volatility model that allows us to examine the impact of volatility through the lens of what is known as a jump diffusion model, which allows to disentangle two kinds of volatility: diffusive (normal shocks) versus jump (large shocks). The paper is trying to test what type of risk were Canadian investors pricing during the March 2020 crash. For that, we calibrate the Bates model on XIU ETF options throughout the March 2020 and we graph the evolution of the parameters of the model. XIU ETF started trading in 1990, making it the first ETF in the world. It

has a large exposure to the biggest Canadian companies, and it aims to replicate the performance of the S&P/TSX 60 index, which is also an index of 60 large companies on the Toronto stock exchange. By comparing the parameters of the diffusion and the jump components, we can get an insight and infer what type of risk was dominant at that time. March 2020 was one of the most volatile months many investors experienced and it would be interesting to see what can the Bates model tell us about the day to day changes the market was experiencing. Option prices reflect the probability of a stock price going above or below a certain level, and through this fundamental idea we can also get a idea of the probability distribution during that time. Was it fat tailed? And if it was, was the distribution positively skewed? In other words, were investors buying more OTM put options to hedge a price decrease hence skewing the distribution to the left or were they not expecting such a drop? Elevated prices in the OTM put options may indicate investors were expecting a drop. A drop in markets can mean two things. A normal drop is what is known as a diffusive risk and generally refers to the daily movement of a stock on a normal day. Jump risk however can mean a sudden drop in the stock price, say from \$30 to \$20 in one day. Many academic journals indicated that this was the dominant type of risk in many markets at that time. We use options on XIU to get an insight on the effect of Covid crisis on Canadian Markets.

**Keywords:** Bates, Characteristic Function, Fast Fourier Transform, Nelder-Mead, Calibration, Jump process.

**Abbreviations:**

- OTM: Out of the money
- ATM: At the money
- ITM: In the money
- GBM: Geometric Brownian Motion
- UA: Underlying Asset

# Contents

<b>1</b>	<b>Introduction</b>	<b>7</b>
<b>2</b>	<b>Literature Review</b>	<b>9</b>
2.1	Impact of Covid-19 on volatility . . . . .	9
2.2	Literature on pricing options using Bates . . . . .	10
<b>3</b>	<b>Methodology</b>	<b>13</b>
3.1	Option Models & Processes . . . . .	13
3.1.1	Poisson Process . . . . .	13
3.1.2	Merton Model . . . . .	14
3.1.3	Bates Model . . . . .	15
3.2	Characteristic Functions . . . . .	16
3.3	Fast Fourier Transform . . . . .	16
3.3.1	CF for Bates . . . . .	19
<b>4</b>	<b>Data &amp; Calibration</b>	<b>21</b>
4.1	Nelson-Siegel model . . . . .	25
4.2	Calibration . . . . .	26
4.3	Fitting Performance . . . . .	27
<b>5</b>	<b>Results</b>	<b>31</b>
<b>6</b>	<b>Conclusion</b>	<b>39</b>

<b>References</b>	<b>41</b>
<b>A Appendix</b>	<b>44</b>
A.1 Deriving the CFs for Affine Diffusion models . . . . .	44
A.1.1 Example using Black Scholes . . . . .	46
A.2 Stochastic Volatility Models . . . . .	48
A.2.1 Cox-Ingersoll-Ross . . . . .	48
A.2.2 Heston Model . . . . .	48
A.3 Varying the Parameters . . . . .	50
A.4 Nelder-Mead Algorithm . . . . .	52

# List of Figures

4.1	Evolution of ETF XIU Price . . . . .	21
4.3	Fits for February 14 . . . . .	28
4.4	Fits for March 4 . . . . .	29
4.5	Evolution of MSE . . . . .	30
5.1	Initial parameters for calibration . . . . .	31
5.2	Calibrated Parameters . . . . .	32
5.3	Diffusion Parameters' Evolution . . . . .	34
5.4	Jump Parameters' Evolution . . . . .	34
A.1	Impact of varying $v_0$ and $\theta$ . . . . .	50
A.2	Varying the jump parameters . . . . .	50
A.3	Varying $\kappa$ . . . . .	51
A.4	Varying vol of vol and $\rho$ . . . . .	51
A.5	Varying $\sigma_J$ . . . . .	51
A.6	Reflection Step . . . . .	52

# Chapter 1

## Introduction

Even though the Black-Scholes (Black & Scholes, 1973) was a huge milestone for what we know now as option pricing, its limitation forced practitioners and academics alike to try and search for other alternatives. One of the limitations we mentioned before is the assumption that implied volatility should be constant across all maturities and strikes. This assumption is clearly violated in practice and we witness varying implied volatilities with respect to both option strikes and maturities. The other assumption is that stock prices follow a log-normal distribution whereas in reality most stock prices have fatter tails than the distribution implies. Many features observed in option pricing cannot describe market behaviors that we currently witness. Alos et al. (2007) argues that while stochastic volatility models can capture volatility smiles for longer maturity, a jump component becomes necessary to have a better fit for the short term smiles. Stochastic volatility models include the Heston (Heston, 1993) which assumes stochastic volatility, and Bates (Bates, 1996) which combines that with the jump component of the Merton model. The arrival of new information can create sudden change in prices, hence adding jumps to the diffusion price dynamics allows a more realistic modelling of the underlying's price behavior. A closed form solution is not available. Hence, alternative methods such as the Monte Carlo Simulation, finite differences, or pricing using the characteristic

function are commonly used. In this paper, we use the latter as our method to fit the Bates model on observed market prices, and the market prices used are the XIU ETF options dating back from January 2020 to March 2020, the month where the crash occurred.

The paper is organized as follows. The literature review elaborates on the global market condition during the time of the pandemic and the impact Covid-19 had on volatility. Literature on pricing various exotics and American options using Bates are presented as well. Data and Methodology section delves deeper on the pricing using Bates, with a focus on the Fast Fourier Transform and the different processes that contribute to the creation of Bates. We explain the characteristic function and its importance in modelling stochastic volatility models when the risk neutral density of the terminal stock price is not available. We also explain the calibration process and the method used for finding the least square error of the objective function. We present our data with some option prices from the period calibrated, and we lastly introduce the method used to find the term structure of interest rates for discounting the options. We then present our results, showing the evolution of our parameters and some random fits from before and after the crisis. The mean of the jump in our model moves from positive (positive jump/movement expectation in the UA price) territory to negative territory on March 12, coinciding with the largest drop in the ETF. This shows that investors were pricing a huge drop before March 12, and expected a rebound in the price afterwards. Diffusive parameters were negligible before March 12, indicating a relatively calm market environment. After the crash, both diffusive and jump were elevated indicating extreme market volatility.

# Chapter 2

## Literature Review

### 2.1 Impact of Covid-19 on volatility

After being the main headline for the past 2 years, the Covid-19 pandemic had a huge toll on market prices, volatility and investor sentiment. In this section, we review the effect of the pandemic on the global stock market and market sentiment in the US. Baker et al. (2020) show that the Covid-19 pandemic had the most significant effect on the stock market compared to other pandemics in 1918–1919, 1957–1958, and 1968. One of the main reasons of this effect is the vulnerability of a service-oriented economy to restrictions on commercial activity. Chatjuthamard et al. (2021) find that when the growth rate of the number of people infected with the virus trends upward, volatility and jumps in the global stock market become more apparent. John and Li (2021) put together proxies for sentiment levels caused by News, Lockdown, Banking, Government relief efforts, and Covid. He finds that the jump component of the VIX index is positively correlated with Market index, Lockdown index, Banking index, and Covid index. Moreover, when the US government announced the relief efforts, that same jump component decreased. Volatility in the energy markets during that time was no different, Shaikh (2022). Li et al. (2021) show the adverse effect the pandemic had on stock market returns of the major affected countries. As

to Europe, Dutillo et al. (2021) show that euro countries' stock markets with large financial centers were more susceptible Covid-19 than the stock market of countries with small financial centers. Moreover, the first wave had the biggest effect on stock market volatility for countries with bigger financial centers. As for commodities, volatility levels in the WTI crude oil market were extremely high. Investors in the energy market were trying to protect themselves from tail risks and paid excess premiums for put options. Li et al. (2021) show that volatility spikes and drops exhibit the same habit among G20 countries during the Covid pandemic. Other findings show that developed markets are usually the main spillover transmitters. Volatility tends to spike in major indices such as the S&P 500 and spillovers to market indices in emerging markets. We can conclude that no financial market on average has not been affected by the pandemic as the trend in most markets were high volatility with lower returns.

## **2.2 Literature on pricing options using Bates**

Commodities in general do exhibit jump-like moves when important news start circulating. Hilliard and Reis (1999) compare the performance of the American version Bates and Black model when used to price soybean futures options. Since the commodity future options studied in the paper are American options, Black and Bates are used alongside the Barone-Adesi and Whaley which is an adjustment used to price American options. The paper reports a Mean Absolute Error (MAE) of 0.0694 for calls and 0.0640 for puts using Bates, whereas 0.2170 and 0.1666 for puts and calls respectively using the Black model. Asian future options are also priced where parameters used to price OTC Asian options are extracted from standard vanilla options. Asian options are exotic options whose payoff is linked to the average of the price of the underlying or the average strikes for a given period of time. They typically are cheaper than vanillas because they average out a collection of prices which

makes the option less volatile. The results on Asian options shows that modelling Asian options using GBM leads to a drastic overpricing in the OTM puts, and underpricing in the OTM Asian Calls. If we compare OTM puts of the same strike, we see that the ratio of prices GBM/Bates surmounts to 4.9269 which is a clear overshooting. The same OTM put had a ratio of 1.7946 for standard vanilla calls. OTM calls for the same strike had a ratio of 1.0164 for Asian options and 1.0483 for vanillas. Using finite differences to price options has been a popular method to price options and can be used to variation of price dynamics that an underlying may exhibit. Finite differences are usually used to price American options due to low dimensionality in pricing an American option. Pricing exotics that exhibit high dimensionalities becomes extremely tedious and becomes computationally costly. Ballestra and Sgarra (2010) propose a method to price American options using finite differences on an underlying modelled by Bates. Early exercise is what differentiates American options on its European counterpart and adding this extra dimension to any pricing method may complicate the derivation. Ballestra and Sgarra (2010) argue that the early exercise component makes it unsuitable to use the characteristic function as a tool for pricing. The early exercise problem is solved by using the Richardson extrapolation of the prices of two bermudian options. Bermudian option are then priced using an implicit/explicit time stepping and a finite element method to arrive at a linear system of equations that can be solved efficiently. All the studies mentioned above show how accurate can Bates be when we try to replicate the price of any type of options. XIU ETF options are European, hence we can, with confidence, be assured that our results should be fairly accurate and as good as any other stochastic volatility model.

Option pricing models are usually used to trade options or to manage one's risk by calculating the Greek parameters and monitoring the evolution of the model's parameters. Barely any literature has been done on the utilization of Bates in the Canadian market, and this paper is here to do exactly that. We use Bates to try to fit

the prices generated from the model with the market prices on the XIU ETF options. We calibrate the model before and after the Covid-19 crash which happened around March. We then decided to calibrate from January 8 until March 24. We could have started calibration on February but we give the model several days to converge to its true parameter values. Bates gives us the chance to decompose volatility into two main components, one being the diffusive volatility which corresponds normal shocks. The other type is jump risk/volatility, known as fat tailed risk. Hence, calibrating Bates allows us to see what type of risk was prevalent at that time, and gives an insight on the day to day trading such an ETF. One might expect an elevation in the jump parameters but the decrease in the price of the XIU was gradual and not sudden. This makes the endeavor more interesting as the results can go either way.

# Chapter 3

## Methodology

### 3.1 Option Models & Processes

Here we delve deeper into the components and processes of the Bates model. The model consists of eight unique parameters which we describe below.

#### 3.1.1 Poisson Process

Dorion and Francois (2021) describes the Poisson process as follows. The standard Poisson process is the stochastic process used to model jumps in models such as the Merton and Bates Model. Stochastic volatility models such as Heston are not able to capture the sudden jumps that an asset can exhibit especially in moments of crises, hence the Poisson process gives us the perfect addition to capture specifically that. The process is denoted by  $N_t$  and is a counting process where a series of events are assumed to be driven by independent and identically distributed random variables that follow an exponential distribution with parameter  $\lambda$  which is commonly referred as the intensity parameter. It is worth mentioning that the Poisson process  $N_t$  is a stochastic process if it satisfies three of the following properties:

- 1) The process starts at 0.
- 2) The process has independent increments. This means that for any  $t$  and  $s$  where

$t > s$ ,  $N_t - N_s$  is independent of  $N_s$

3) An exponentially distributed increments, for any  $n$ , are described by

$$\mathbb{P}(N_t - N_s = n) = \frac{\lambda(t-s)^n}{n!} e^{-\lambda(t-s)} \quad (3.1)$$

### 3.1.2 Merton Model

The Merton model is an extension of the Black-Scholes model as it adds the jump component to try capturing a steep rise or fall in the underlying's price when investors receive new sudden information. By combining the diffusion and Poisson process, we arrive at the following Merton model equation:

$$\frac{dS(t)}{S(t)} = (r - q - \lambda\mu_J)dt + \sigma dW_t + (e^J - 1)dN_t \quad (3.2)$$

where the log-jumps have the distribution:

$$\log(1 + J_t) \sim N(\log(1 + \mu_J) - \frac{v_J}{2}, v_J) \quad (3.3)$$

It is assumed that the correlation between the diffusion and jump process is null.  $\lambda$  is the intensity of the jumps,  $J_t$  is the jump size,  $\mu_J$  and  $v_J$  are the mean and variance of the jump respectively. The skewness of the underlying's distribution is directly affected by  $\mu_J$  whereas the  $v_J$  is more related to the kurtosis. Note that adding the jump component makes the model incomplete, hence we do not have a unique risk-neutral measure that makes the discounted price of the underlying a martingale.

### 3.1.3 Bates Model

The Bates model adds another layer to the Merton model by assuming that volatility is stochastic. One could also argue that Bates is just a Heston model <sup>1</sup> with a jump process which is just another way of looking at the model. Volatility of the underlying is assumed to follow a mean reverting process, following the Cox–Ingersoll–Ross model. The price of the underlying and its variance is characterized by

$$dS_t = (r - q - \lambda\mu_J)S_t dt + \sqrt{V_t}S_t dW_t + J_t S_t dN_t \quad (3.4)$$

$$dV_t = \kappa(\theta - V_t)dt + \sigma\sqrt{V_t}dZ_t \quad (3.5)$$

The model assumes a correlation between the diffusion processes of the underlying and its variance

$$dW_t dZ_t = \rho dt \quad (3.6)$$

$\theta$  is the long term variance, and it is worth mentioning that both  $\theta$  and  $\rho$  have the same impact on the implied volatility of the option, and is usually negative, which is what we typically see in real market observations, Cont (2001). The negative correlation between the asset's price or returns to its volatility is known as the 'leverage effect'.  $\kappa$  is the speed of mean reversion, and has a lesser effect on the implied volatility smile when compared to the other parameters.  $\sigma$  is the volatility-of-volatility, and it gives our implied volatility surface a more steeper skew. The jump components produces a higher implied volatility than the ones implied by Heston especially in the short end, giving us better chances to fit market data <sup>2</sup>.

---

<sup>1</sup>More on Heston and CIR in the appendix.

<sup>2</sup>The effects of the parameters on the volatility smile is shown graphically in the appendix.

## 3.2 Characteristic Functions

Characteristic functions is a mirror image of a probability density function as it contains the probability distribution of the underlying asset at any point in time. For our case, the characteristic function is known analytically. According to Bakshi and Madan (2000), European options are priced by the following formula:

$$C_0 = e^{-q\tau} S_0 \Pi_1 - e^{-r\tau} X \Pi_2 \quad (3.7)$$

On the other hand, the risk-neutral probability of the option finishing in the money is:

$$P(S_T > K) = \Pi_2 = \frac{1}{2} + \frac{1}{\pi} \int_0^\infty \operatorname{Re} \left( \frac{e^{-iu \ln K} \phi_T(u)}{iu} \right) du \quad (3.8)$$

with delta being

$$\Delta_1 = \frac{1}{2} + \frac{1}{\pi} \int_0^\infty \operatorname{Re} \left( \frac{e^{-iu \ln K} \phi_T(u - i)}{iu \phi_T(-i)} \right) du \quad (3.9)$$

## 3.3 Fast Fourier Transform

Carr and Madan (1999) developed an algorithm that computes the price of an option using what is known as the Fast Fourier Transform. The advantages of pricing using FFT is its speed and ability to price options for a wide range of given strikes. Moreover, the characteristic options for many stochastic volatility models are known, whereas their density is in most cases not available. Borak et al. (2005) explain that the goal of this method is to develop a Fourier transform expression as a function of the call price, and then inferring the price by Fourier inversion. The standard call premium  $C_T(k)$  is described by the following equation:

$$C_T(k) = \int_k^{+\infty} e^{-rT} (e^s - e^k) q_T(s) ds \quad (3.10)$$

where  $K$  is the log price of the strike  $K$ , and  $q_T$  is the density of  $s_T = \log S_T$  under the risk neutral measure. The general characteristic function that pertains to  $s_T$  is defined by

$$\phi_T(u) = \int_{-\infty}^{+\infty} e^{ius} q_T(s) ds \quad (3.11)$$

There is a slight modification that Carr and Madan (1999) do to transform equation 3.10 to a square-integrable function

$$c_T(k) = e^{\alpha k} C_T(k) \quad (3.12)$$

where  $\alpha$ , also known as the damping factor, is recommended to be strictly positive. The equation is just an adjustment to the call price  $C_T(k)$  made by Carr and Madan. We will be using the adjusted call price  $c_t(k)$  in the equations below.

The expression for the characteristic function can now be easily inferred:

$$\begin{aligned} \phi_T(v) &= \int_{-\infty}^{+\infty} e^{ivk} \int_k^{+\infty} e^{\alpha k} e^{-rT} (e^s - e^k) q_T(s) ds dk \\ &= \int_{-\infty}^{+\infty} e^{-rT} q_T(s) ds \int_{-\infty}^s (e^{\alpha k+s} - e^{(\alpha+1)k}) e^{ivk} dk ds \\ &= \int_{-\infty}^{+\infty} e^{-rT} q_T(s) \left( \frac{e^{(\alpha+1+iv)s}}{\alpha + iv} - \frac{e^{(\alpha+1+iv)s}}{\alpha + 1 + iv} \right) ds \\ &= \frac{e^{-rT} \phi_T(v - (\alpha + 1)i)}{\alpha^2 + \alpha - v^2 + i(2\alpha + 1)v} \end{aligned} \quad (3.13)$$

Using the inverse transform and by substituting, we get the option price in terms of the characteristic function

$$C_T(k) = \frac{e^{-\alpha k}}{\pi} \int_0^{+\infty} e^{-ivk} \phi(v) dv \quad (3.14)$$

The above equation can be written, by utilising the trapezoid rule for integration

on the integral part of equation 3.14, and by setting  $v_j = \nu j$  for  $j = 0, \dots, N - 1$ , as

$$C_T(k) \approx \frac{e^{-\alpha k}}{\pi} \sum_{j=0}^{N-1} e^{-iv_j k} \phi(v_j) \nu \quad (3.15)$$

The generic FFT method computes the sum of

$$w(k) = \sum_{j=0}^{N-1} e^{-i\frac{2\pi}{N}(j-1)(k-1)} x(j), \text{ for } k = 0, \dots, N - 1 \quad (3.16)$$

$N$  here is a power of 2. The main reason why the FFT method is considered fast and efficient is because it reduces the computation from  $N^2$  to  $N \log N$ , which reduces computational time by quite a lot. This FFT algorithm will allow us to compute the summation of equation 3.15. Carr and Madan suggested an integration method known as the Simpson rule which transforms our pricing equation to the following

$$C(k_u) = \frac{e^{-\alpha k_u}}{\pi} \sum_{j=0}^{N-1} e^{-i\frac{2\pi}{N}(j-1)(u-1)} e^{ibv_j} \phi(v_j) \frac{\nu}{3} [3 + (-1)^j - \delta_{j-1}] \quad (3.17)$$

The Kronecker delta function  $\delta_{j-1}$  is a binary function where it takes 1 for  $n = 0$  and 0 otherwise. Based on FFT convention, we have decided to take  $\alpha = 1.5$  and  $\nu = .25$  as they have been proven to be the best values where the option converges to its true value.

Density functions for some stochastic variables in literature is known, and from that we deduce probabilities, expectations and variances which then allows us to price our instrument. Characteristic functions are used when the density function of our variable is not defined which is the case with the Bates model. Fast Fourier transform is one of various techniques that use the characteristic function as a technique to price options and due to its simplicity and speed, we have decided to use it to price the XIU options.

### 3.3.1 CF for Bates

One can decompose the characteristic function of Bates as being the addition of the CF of Heston and the CF of Merton.<sup>3</sup> Albrecher et al. (2007) define the characteristic function of Bates as follows:

$$\phi = e^{A+B+C+D} \quad (3.18)$$

$$A = i\omega \log S_0 + i\omega(r - q)\tau$$

$$B = \frac{\theta\kappa}{\sigma^2}(\kappa - \rho\omega - d)\tau - 2\log\left(\frac{1 - ge^{-d\tau}}{1 - g}\right)$$

$$C = \frac{v_0}{\sigma^2} \left( \frac{(\kappa - \rho\omega - d)(1 - e^{-d\tau})}{1 - ge^{-d\tau}} \right)$$

$$D = -\lambda_j \mu_j i\omega\tau + \lambda\tau \left( (1 + \mu_J)^{i\omega} e^{\frac{1}{2}v_J i\omega(i\omega-1)} - 1 \right)$$

$$d = \sqrt{\rho\sigma i\omega^2 + \sigma^2(i\omega + \omega^2)}$$

$$g = \frac{\kappa - \rho\omega - d}{\kappa - \rho\omega + d}$$

---

<sup>3</sup>More on CFs in the appendix.

It is important to mention that even though Bates does a better job in capturing the short end of the skew, there is one main limitation worth mentioning. The Bates model has 8 distinct parameters with many of those having the same effect on the implied volatility, hence many of those parameters can in fact be correlated, which may put us at a risk of over fitting.

# Chapter 4

## Data & Calibration

Data used for this paper is the XIU ETF options. We calibrate the months of January, February and March of 2020. On March 11, the closing price was 21.46, on the 12th it dropped to 18.83, rebounds the next day to 20.82, and then drops again on March 16 to 18.76. The real drop in the price of the ETF was on March 12 and the trough was around 18.83. So, the goal is to calibrate before and after the drop and monitor our parameters. Figure 4.1 is a graph that shows the drop:



Figure 4.1: Evolution of ETF XIU Price

In order to get a consistent parameter evolution that reflect market conditions before the drop, we calibrate the parameters from January 8. The ETF has the most liquidity for options around the money, and the table below is the prices for the options on January 9, with a maximum maturity close to one year. The decision to remove higher maturity options is due to the lack of liquidity. The contribution would be very minimal and they might bias our parameters. We also remove bid prices that are zero since they do not really reflect market demand and supply. We also remove prices of put options to make our calibration faster. We assume that put-call parity holds for our data, hence we remove prices of put options to fasten the calibration process. Note that the put call parity in our data does not always hold, especially for options with little to no liquidity. We had to make this assumption since adding data for puts will make the calibration process really time consuming. For March, we have 9330 calls and 9309 puts, the average time to calibrate the parameters on calls only for one day in March was around an hour. Since we are calibrating daily for 2 months (January, February and March) we used this assumption to have an overall view about the Canadian market and the ETF at that time without imposing an unordinary assumption.

We present two sets of data, one from January 9 and the other from March 16. We then present some statistics on the data based on moneyness and maturities. We chose January 9 and March 16 to see the differences before and after the crisis.

Table 4.1: Jan.9 -Data based on Moneyness

	Deep ITM	ITM	OTM	Deep OTM
Total Quotes	8	94	58	12
Max Price	7.91	7.91	2.92	0.455
Min Price	5.9	1.12	0.5	0.05
Mean	6.475	3.01	0.651	0.175
Standard Deviation	0.679	1.565	0.553	0.117

Table 4.2: Jan.9 -Data based on Maturities

	3 months	Between 3-6 months	More than 6 months
Total Quotes	96	17	39
Max Price	6.9	5.90	7.91
Min Price	0.06	0.05	0.065
Mean	1.874	2.387	2.572
Standard Deviation	1.385	1.931	2.179

Table 4.3: Jan.9 -Total Call options

Total Quotes	Max Price	Min Price	Mean	Standard Deviation
152	7.91	0.05	2.111	1.716

Table 4.4: Mar.16 -Data based on Moneyness

	Deep ITM	ITM	OTM	Deep OTM
Total Quotes	6	73	205	49
Max Price	4.225	4.225	2.065	0.51
Min Price	3.28	1.42	0.055	0.055
Mean	3.782	2.552	0.750	0.302
Standard Deviation	0.341	0.586	0.463	0.1

Table 4.5: Mar.16 -Data based on Maturities

	3 months	Between 3-6 months	More than 6 months
Total Quotes	188	28	50
Max Price	3.46	4.16	4.225
Min Price	0.145	0.055	0.12
Mean	1.313	1.20	0.929
Standard Deviation	0.855	1.169	1.025

Table 4.6: Mar.16 -Total Call Options

Total Quotes	Max Price	Min Price	Mean	Standard Deviation
278	4.225	0.055	1.223	0.936

For January 9, the price of the ETF was 25.87. We consider a call with strike between 30.5 and 31 (maximum strike value) as deep OTM, and a call with strike ranging from 20.5 to 18 to be deep ITM. As for March 16, Deep OTM was considered to have a strike range between 31 and 32 and Deep ITM having a range between 14

and 15. The price at that time was 17.71. One thing we immediately notice is that the number of quotes increased sharply after the crisis. This is expected as investors usually find more opportunity during turbulent times and tend to invest more. The total number of quotes varies around the 100-200 range everyday throughout our entire sample of two months which is relatively small compared to indices such as S&P 500, and should be taken into consideration.

## 4.1 Nelson-Siegel model

Discounting is a crucial part of option pricing. We used yields from Canadian treasury bills with maturity up to 3 years. To capture the term structure needed for discounting, we use the Nelson-Siegel model which is used to capture different shapes of the term structure and works relatively well for the short term of the term structure which is what we need since our options have a maximum maturity of 1 year. The following is the Nelson-Siegel equation used to model the forward term structure:

$$f(0, T_i) = \beta_0 + \beta_1 e^{-\frac{T_i}{\theta}} + \beta_2 \frac{T_i}{\theta} e^{-\frac{T_i}{\theta}} \quad (4.1)$$

The first and the second term of the equation tries to capture different shapes of the interest rate term structure. Many academics add a third term to better capture the long end of the term structure but since we use interest rates up to three years, we limit our equation to the first two terms. The following relationship between the continuous spot and forward rates is:

$$R(0, T_i) = \frac{1}{T_i} \int_0^{T_i} f(0, s) ds \quad (4.2)$$

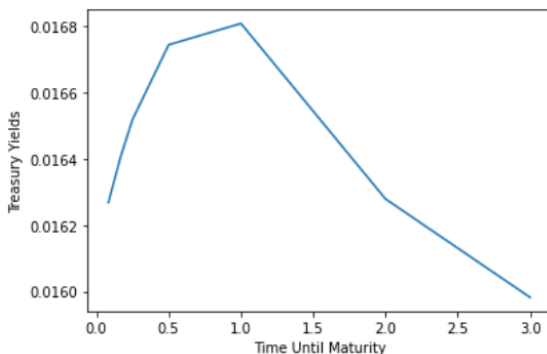
Replacing (3.20) into (3.19):

$$R(0, T_i) = \beta_0 + \beta_1 \left( \frac{1 - e^{-\frac{T_i}{\theta}}}{\frac{T_i}{\theta}} \right) + \beta_2 \left( \frac{1 - e^{-\frac{T_i}{\theta}}}{\frac{T_i}{\theta}} - e^{-\frac{T_i}{\theta}} \right) \quad (4.3)$$

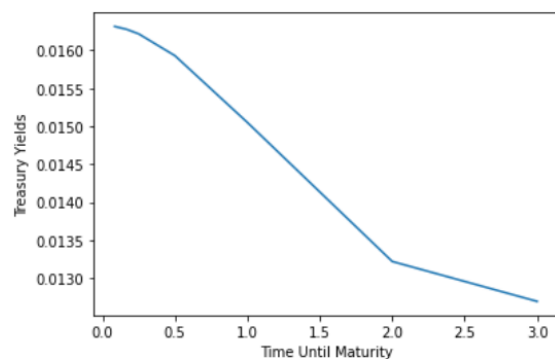
We then calibrate the rates generated by Nelson-Siegel with market rates using the following equation:

$$\min_{\phi} \sum_{i=1}^{\alpha} (R(0, T_i)_{market} - R(0, T_i)_{NS})^2 \quad (4.4)$$

where  $\phi = \beta_0, \beta_1, \beta_2, \theta$ .  $\alpha$  is the last maturity date of our term structure. Figures (a) and (b) shows the term structure for up to three years. Even though time to maturity is limited to three years, there clearly is an inversion in the term structure which may have been a signal to what is coming.



(a) Jan 20 Term Structure



(b) March 12 Term Structure

## 4.2 Calibration

Calibrating model prices to market ones is not a simple task especially if you have a relatively large number of parameters. Many practitioners prefer a low set of parameters to avoid noise and overfitting. Before describing our calibration method, we should highlight the limitations of calibrating a model such as Bates. Eight parameters are needed to be calibrated,  $\omega = \kappa, \theta, \sigma, v_0, \rho, \lambda_J, \mu_J, \sigma_J$ , and many of them have the same impact on the volatility smile. This increases the risk of overfitting, and even though we may have the ability to fit all sort of structures, the ability to forecast with such a model may be dampened. This may also cause the objective function not to be as smooth as one might want it to be, hence we might encounter several local minima. As for the objective function, we are looking for

model parameters that minimizes the differences between model call prices  $C_{Bates}$  and market call prices  $C_{mkt}$ . The minimization is solved as a non-linear least squares optimization problem. For  $\omega = \kappa, \theta, \sigma, v_0, \rho, \lambda_J, \mu_J \sigma_J$ :

$$MSE = \frac{1}{N} \min_{\omega} \sum_{i=1}^N (C(K_i, T_i)_{mkt} - C(K_i, T_i)_{Bates})^2 / C(K_i, T_i)_{Bates} \quad (4.5)$$

where  $N$  corresponds to the number of XIU call options.

### 4.3 Fitting Performance

The following are the fits for February 14 and March 4 for random maturities. Maturities are mentioned on the top of the graph. The blue curve corresponds to market prices whereas the yellow one is the prices generated by Bates.

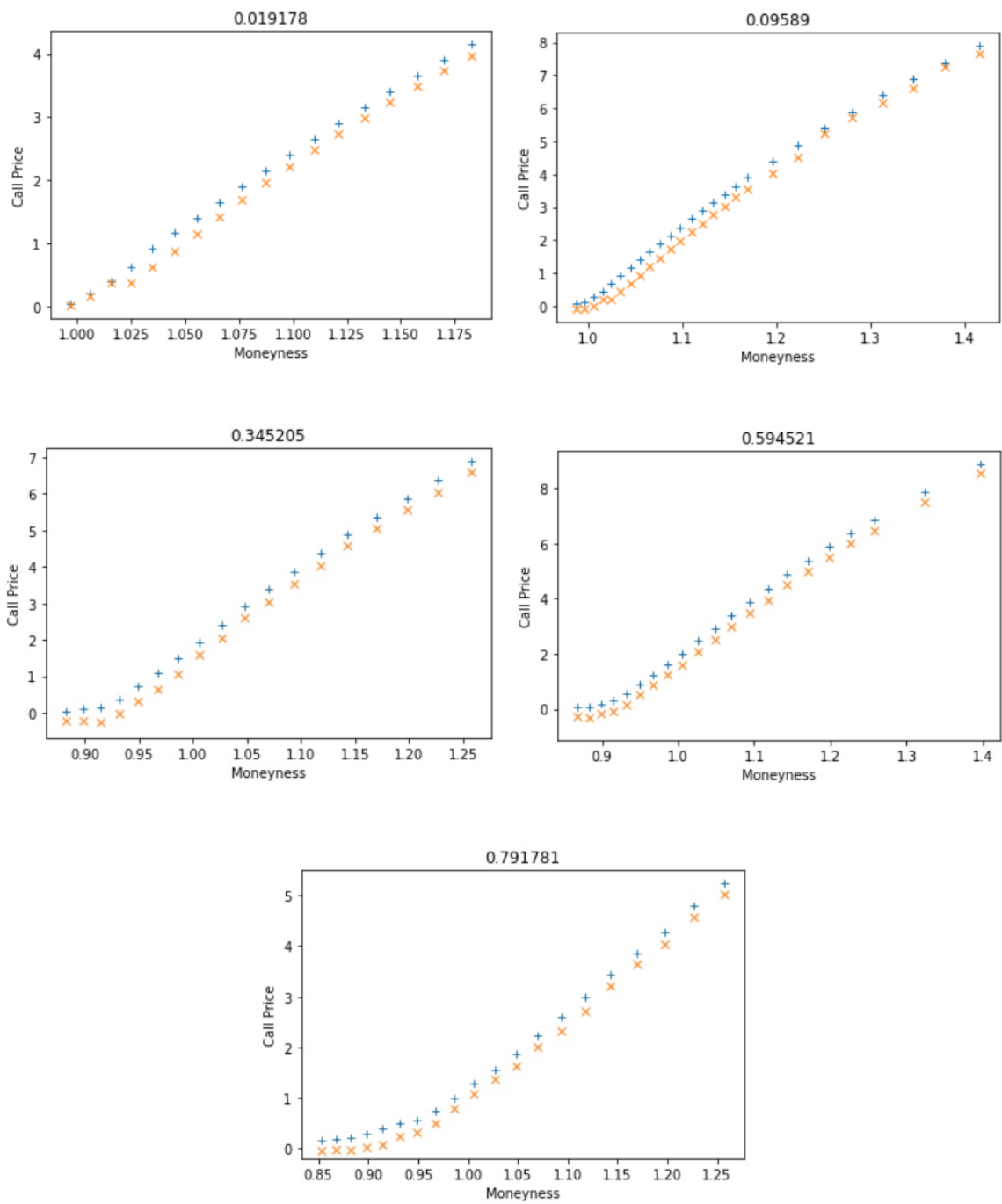


Figure 4.3: Fits for February 14

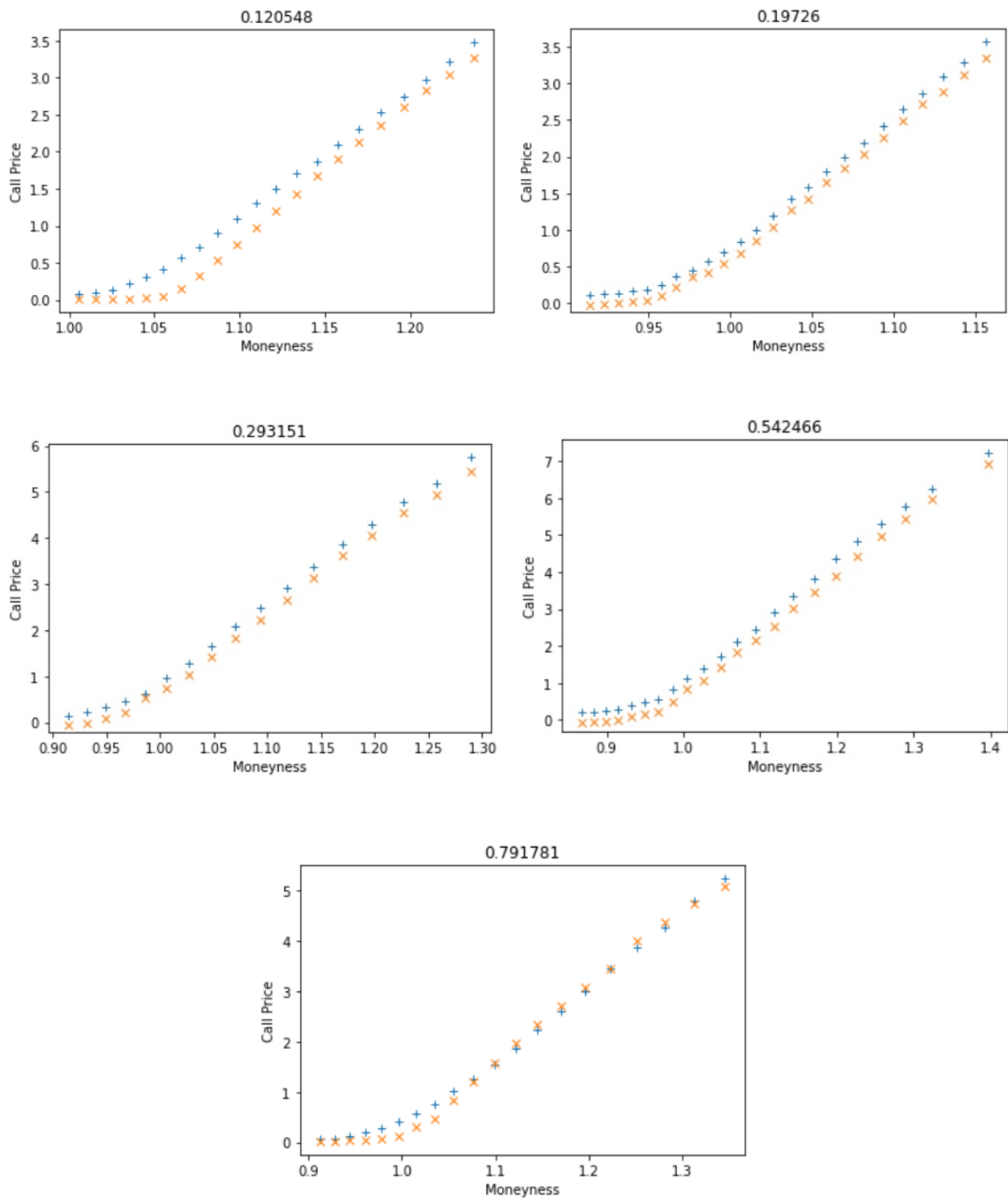


Figure 4.4: Fits for March 4

On the other hand, the mean square error was as follows. The error was really close to zero before the crisis, but increased a bit after the crisis and the worst fit was on the day of the second largest drop in March 16, where the MSE was equal to 0.103708. This high error was expected as the market was really volatile and fear

at that time may change the normal market dynamics that the model can usually capture. There might have been a regime change which the Bates model cannot capture, hence we see an elevation towards the end of the March.

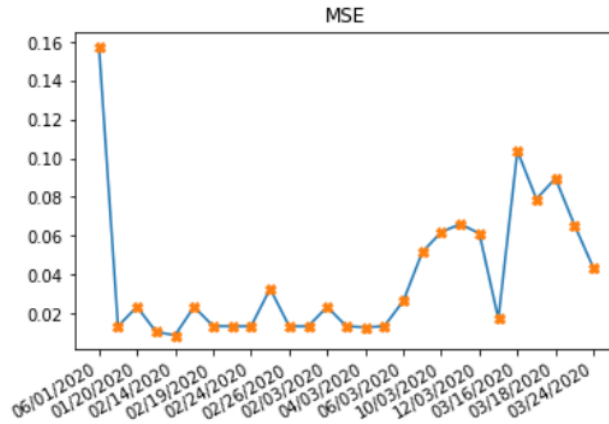


Figure 4.5: Evolution of MSE

This graph shows exactly why we decided to start two months before the crisis. Even though we did not calibrate on every day in January, we gave the model a learning time-frame so that it can converge to its true parameters. For January, we calibrated the model on January 7,8,13,20 and 28. We use the parameters of the previous day to calibrate the parameters of the next. For example, after putting in an initial parameter guess and calibrating on the 8th of January, we use the calibrated parameters as an initial guess for the 9th and so on. We use previous points as starting values because we believe values on the previous day should be a reasonable estimate to the day after. Unless we face a moment of crisis like the one on March 12-16, our parameters change within a reasonable range. The reason why we do not calibrate for every single day in January is that after the 13th of January we notice that the parameters stabilize around certain values. This is clear in the parameter evolution graphs presented in the section below. February happens to be the month with the least errors and calibrating several days in January really helped reach these small values. We calibrate the whole month of February and March until we reach March 24.

# Chapter 5

## Results

The first day of calibration was on January 7 and to start, we ran the computation using the following initial parameters:

Initial Parameters	
Mean reversion $\kappa$	0.01
Long-term mean of variance $\theta$	0.019
Volatility of the volatility $\sigma$	0.033
Correlation between Brownian Motions $\rho$	-0.7
Variance initial value $V_0$	0.0724
Jump intensity $\lambda_J$	0.59
Jump mean $\mu_J$	-0.04
Jump volatility $\sigma_J$	0.06

Figure 5.1: Initial parameters for calibration

We chose  $\lambda_J$  to be 0.59 as per Lindström et al. (2008). Most of the literature has relatively high values for kappa but after shocking the parameters, we found that kappa in our case should be anywhere between 0.09 and 0.01. The jump parameters were also used from Lindstrom's paper while the others were changed manually,

before calibration, to get the least mean squared error. We start with a  $\mu_J$  of zero. A negative  $\mu_J$  means that the underlying is expected to have more downward jumps whereas a positive jump mean indicates the opposite. As for the initial value for  $v_0$ , we use the following heuristic method by Oosterlee and Grzelak (2019). For a maturity close to zero, one might expect the underlying to follow the Geometric Brownian motion process:

$$dS(t) = rS(t)dt + \sqrt{v_0}S(t)dW(t) \quad (5.1)$$

We can approximate  $T \rightarrow 0$  by an option with the shortest maturity. This implies that  $v_0$  can be approximated by the square of the short maturity ATM implied volatility,  $v_0 \approx \sigma_{imp}^2$ , Yan (2011).

Calibrated parameters for that day gave us the following result:

Initial Parameters	
Mean reversion $\kappa$	0.01001
Long-term mean of variance $\theta$	0.02239
Volatility of the volatility $\sigma$	0.03985
Correlation between Brownian Motions $\rho$	-0.8231
Variance initial value $v_0$	0.785
Jump intensity $\lambda_J$	0.125
Jump mean $\mu_J$	0
Jump volatility $\sigma_J$	0.072

Figure 5.2: Calibrated Parameters

It is important to mention the boundaries that we have set throughout the calibration process. The boundaries clearly affect the results and it should be mentioned that we force vol of vol  $\sigma_J$ , and jump intensity  $\lambda_J$  to be non-negative and correlation

$\rho$  to vary from 1 to -1.  $\theta$ ,  $v_0$ ,  $\sigma_J$ ,  $\kappa$  are also set to be non-negative. We also try to increase or decrease the boundaries of other parameters so that the optimization takes less time. An example of this would be setting  $\kappa$  anywhere between 0.01 and 0.09, or setting vol of vol to range from 0.01 to 0.1 before the crisis as this was generally what many would consider a reasonable range for a calm market.

The reason why we presented the initial parameters is to highlight the importance of choosing a set of parameters that can closely match the ETF price. This importance stems from the fact that the Nelder-Mead works optimally when one feeds it a reasonable set of initial parameters especially if the model has a large number of them. We stopped the daily calibration at March 24, and we notice the volatility of the ETF price is relatively minimal as the price stabilizes around \$20 at that time. Moreover, many practitioners refer to March 2020 as the month where the crash happened. We present the evolution of the parameters in the following figures. As one can notice, March 12 and March 16 were the days where our parameters change the most, and this is expected as the two largest drops were on those two days, with around 12 and 9 percent drop respectively. Note that we only have one trading day between the two, March 13, which happens to be on a Friday.

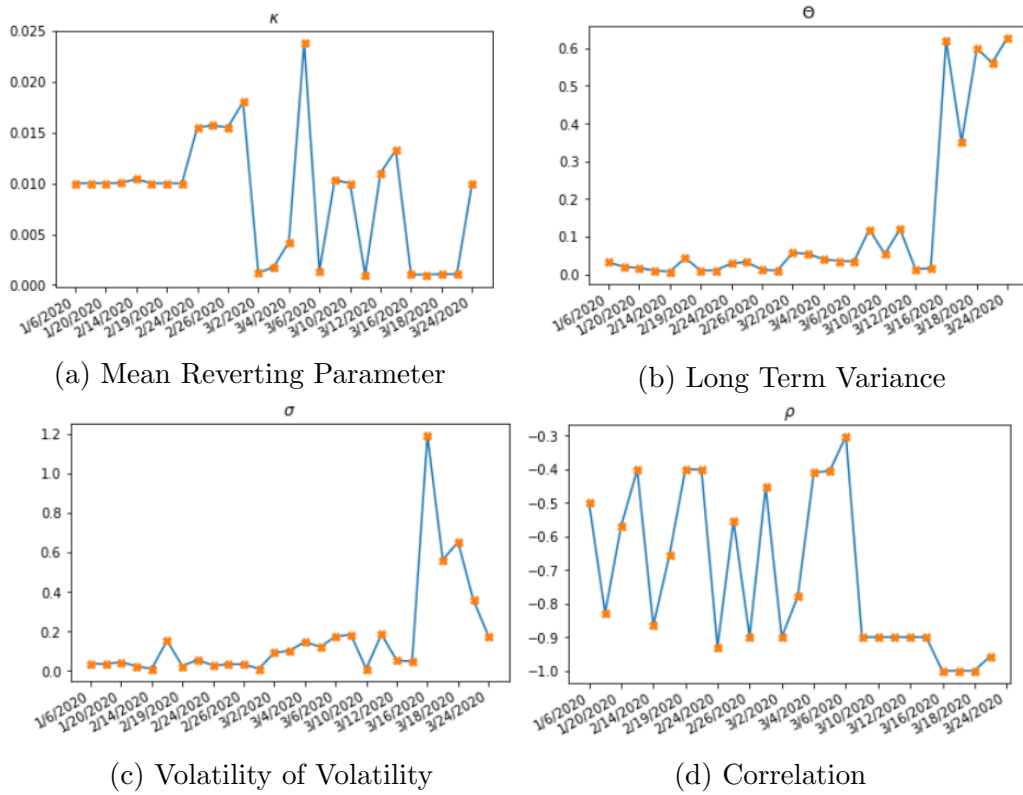


Figure 5.3: Diffusion Parameters' Evolution

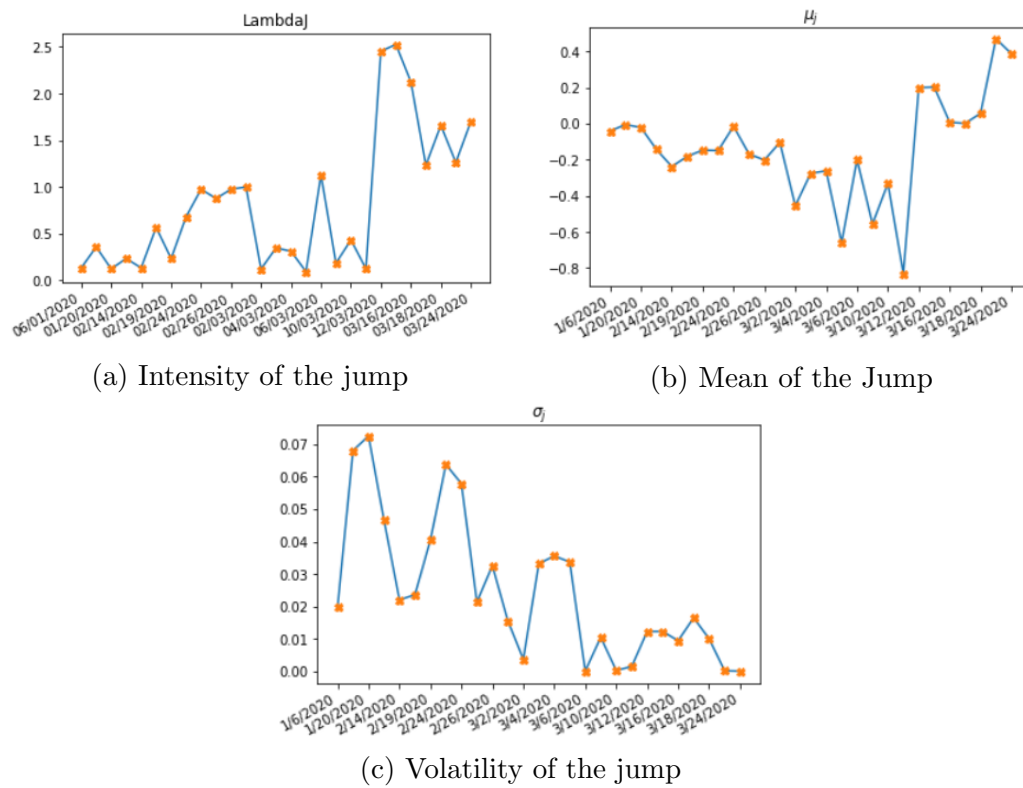


Figure 5.4: Jump Parameters' Evolution

Kappa does not exhibit any movement and does not really have that of an effect on the smile. Theta and sigma almost exhibit a similar pattern. They were low throughout January, February and early March but spike around the 16th of March. The parameters above and the move in the underlying clearly proves that the peak of the crisis was on March 16. On the 16th, the mean of the jump moves from negative to positive territory. One might ask what happened on March 16 for our parameters to exhibit such behavior. This behavior resembles a combination of diffusion and jump processes where the price of the underlying moves up and down, with large and sharp deviations causing a spike in volatility, theta, and the mean of the jump. The mean of the jump at January 8 starts around zero (slightly positive), which is what we expect in a calm market like the one in January. As we get closer to March, the mean decreases steadily and stabilizes in the negative region before exhibiting a large drop on March 16th. On this day, the ETF makes its second largest drop of 8 percent after dropping another 12 percent 2 trading days before on the 12th. This causes the mean of the jump to steeply decrease to around -0.8. What is interesting is that after this drop, the mean of the jump increases dramatically to fall within the positive territory, indicating that the market was pricing in a sudden increase towards the upside after this drop. This also coincides with a spike in the intensity of the jump on the same date as well. The evolution of the parameters indicate that around the beginning of March, the market was pricing in a jump-like negative drop in the ETF. After the drop happened twice on the 12th and 16th, the market priced in a jump upwards with sharp deviations in the price. We then can divide the three tested months into three distinct three periods. The period between the first day of calibration and February 3th would be characterized as period of a calm market with neither jump nor diffusion parameters exhibiting any non-ordinary behavior. After February 3, we witness the first drop in the mean of the jump from positive to negative territory indicating that the market was starting to price in a sharp price reduction. The jump of the mean kept decreasing up until March 16 with

little to any movement in the diffusion parameters. The market was pricing in a sudden drop in price, and after that drop happened, we witness a sharp rise in the diffusion parameters, mainly theta and volatility of volatility, with the jump of the mean moving to positive territory, and the intensity of the jump sharply rising. This period up until the last day of calibration had both high jump and diffusion parameter values, indicating that the market was expecting both a high volatility in the price of the ETF and a sharp rise to the upside, mainly a rebound to the largest drop in the ETF's price on March 12.

Table 5.1: Parameter Mean & Standard Deviation

Parameters	Mean	Standard Deviation
$\kappa$	0.008786526	0.006129671
$\theta$	0.131051406	0.211485298
$\sigma$	0.167903976	0.26005385
$\rho$	-0.719398809	0.240885041
$\lambda_J$	0.547454854	1.087923011
$\mu_J$	-0.135204116	0.286273436
$\sigma_J$	0.024554721	0.021850588

This table gives us an overall picture of what we saw in the graphs. The highest deviations from the mean were from the diffusion and the jump parameters, with the intensity of the jumps getting the highest value. We also notice a negative average for the mean of the jumps, which indicates that during that time, market sentiment was expecting, on average, a sharp drop in the price of the ETF. We also present the mean and standard deviations of the parameters before March 12 and after March 12 where every sample contains 8 calibrated days.

Table 5.2: Before Mar.12 parameter Mean &amp; Standard Deviation

Parameters	Mean	Standard Deviation
$\kappa$	0.009922378	0.006752116
$\theta$	0.041763639	0.034709636
$\sigma$	0.084754986	0.067118278
$\rho$	-0.66569351	0.239823888
$\lambda_J$	0.697801444	0.445102649
$\mu_J$	-0.298029114	0.219813854
$\sigma_J$	0.02471375	0.019494354

Table 5.3: After Mar.12 parameter Mean &amp; Standard Deviation

Parameters	Mean	Standard Deviation
$\kappa$	0.005490512	0.005632359
$\theta$	0.398741668	0.278633641
$\sigma$	0.434304222	0.410635061
$\rho$	-0.959373333	0.049013838
$\lambda_J$	0.673217903	1.916143115
$\mu_J$	0.189619339	0.18452323
$\sigma_J$	0.008657202	0.006280627

Before March 12, theta and sigma were pretty low whereas the mean of the jump had was deeply negative. This indicates that the market was pricing in a jump downwards with little small deviations. After March 12, theta and sigma sharply rose in value and the mean of the jump went to positive territory indicating a change in market sentiment. Now the market was pricing heavy deviations with a shock to the upside. In other words, the expectation was that the price will move like a

combination of a jump and diffusion process.

# Chapter 6

## Conclusion

In this paper, we try to test how the Canadian market reacted to Covid crisis of March using XIU ETF options. The ETF includes major Canadian financial and construction companies and could be perceived as a good representation of the Canadian stock market. To test the reaction of that market, we use the Bates model, which is a stochastic volatility model that allows us to examine the disentangle two kinds of volatility: diffusive (normal shocks) versus jump (large shocks). We use the Characteristic function approach to model Bates, and to fasten the time needed to generate prices, we use Fast Fourier Transform. We calibrate the model on the market prices using the Nelder-Mead optimizations from January 7 till March 24. The results clearly show an elevation in the jump parameter, especially the mean of the jump. One of the more interesting finds were on March 16, where the mean of the jump went suddenly from the negative to positive territory, indicating a price jump to the upside, in addition to a rise in the diffusion parameters, which was not what we expected. The peak of the crisis was on the 16th where we witnessed the second largest drop in the ETF, the largest being on the 12th, two trading days before. The evolution of the parameters reconfirms exactly that, and we see drastic changes in the value of the parameters after that date. March 2020 was an exceptional time for markets so seeing these type of results should not come as a real surprise.

Our calibration error started to rise a bit after March 16 for reasons that can be explored in later research. We used the local optimization technique, Nelder Mead, which may not be sufficient to capture a surface with several global minimums, and that might be the reason why we have a relatively high MSE during that time. One could say that there might have been a regime change during that time which the model cannot capture, and we leave this problem for future research.

# References

- Albrecher, H., Mayer, P., Schoutens, W., & Tistaert, J. (2007). The little heston trap. *Wilmott*(1), 83–92.
- Alos, E., León, J. A., & Vives, J. (2007). On the short-time behavior of the implied volatility for jump-diffusion models with stochastic volatility. *Finance and Stochastics*, 11(4), 571–589.
- Baker, S. R., Bloom, N., Davis, S. J., Kost, K., Sammon, M., & Viratyosin, T. (2020, 07). The Unprecedented Stock Market Reaction to COVID-19. *The Review of Asset Pricing Studies*, 10(4), 742-758.
- Bakshi, G., & Madan, D. (2000). Spanning and derivative-security valuation. *Journal of Financial Economics*, 55(2), 205-238.
- Ballestra, L. V., & Sgarra, C. (2010). The evaluation of american options in a stochastic volatility model with jumps: An efficient finite element approach. *Computers & Mathematics with Applications*, 60(6), 1571–1590.
- Bates, D. S. (1996). Jumps and stochastic volatility: Exchange rate processes implicit in deutsche mark options. *The Review of Financial Studies*, 9(1), 69–107.
- Black, F., & Scholes, M. (1973). The pricing of options and corporate liabilities. *Journal of political economy*, 81(3), 637–654.
- Borak, S., detlefsen, K., & Härdle, W. K. (2005, 04). Fft-based option pricing. doi: 10.1007/3-540-27395-6\_8
- Carr, P., & Madan, D. (1999). Option valuation using the fast fourier transform.

- Journal of computational finance*, 2(4), 61–73.
- Chatjuthamard, P., Jindahra, P., Sarajoti, P., & Treepongkaruna, S. (2021). The effect of covid-19 on the global stock market. *Accounting & Finance*, 61(3), 4923–4953.
- Cont, R. (2001). Empirical properties of asset returns: stylized facts and statistical issues. *Quantitative finance*, 1(2), 223.
- Duffie, D., Pan, J., & Singleton, K. (2000). Transform analysis and asset pricing for affine jump-diffusions. *Econometrica*, 68(6), 1343–1376.
- Duttilo, P., Gattone, S. A., & Di Battista, T. (2021). Volatility modeling: An overview of equity markets in the euro area during covid-19 pandemic. *Mathematics*, 9(11).
- Gao, F., & Han, L. (2012). Implementing the nelder-mead simplex algorithm with adaptive parameters. *Computational Optimization and Applications*, 51(1), 259–277.
- Heston, S. L. (1993). A closed-form solution for options with stochastic volatility with applications to bond and currency options. *The review of financial studies*, 6(2), 327–343.
- Hilliard, J. E., & Reis, J. A. (1999). Jump processes in commodity futures prices and options pricing. *American Journal of Agricultural Economics*, 81(2), 273–286.
- John, K., & Li, J. (2021). Covid-19, volatility dynamics, and sentiment trading. *Journal of Banking Finance*, 133, 106162.
- Li, Y., Zhuang, X., Wang, J., & Dong, Z. (2021). Analysis of the impact of covid-19 pandemic on g20 stock markets. *The North American Journal of Economics and Finance*, 58, 101530.
- Lindström, E., Ströjby, J., Brodén, M., Wiktorsson, M., & Holst, J. (2008). Sequential calibration of options. *Computational Statistics & Data Analysis*, 52(6), 2877–2891.
- Oosterlee, C. W., & Grzelak, L. A. (2019). *Mathematical modeling and computa-*

*tion in finance: with exercises and python and matlab computer codes.* World Scientific.

Shaikh, I. (2022). Impact of covid-19 pandemic on the energy markets. *Economic Change and Restructuring*, 55(1), 433–484.

Singer, S., & Singer, S. (2004). Efficient implementation of the nelder–mead search algorithm. *Applied Numerical Analysis & Computational Mathematics*, 1(2), 524–534.

Yan, S. (2011). Jump risk, stock returns, and slope of implied volatility smile. *Journal of Financial Economics*, 99(1), 216–233.

# Appendix A

## Appendix

### A.1 Deriving the CFs for Affine Diffusion models

Oosterlee and Grzelak (2019) define an Affine Diffusion process as follows. Suppose you have state variables that have the following SDEs:

$$dX(t) = \bar{\mu}(X(t))dt + \bar{\sigma}(X(t))dW(t) \quad (\text{A.1})$$

Assuming the brownian motions are independent, for a process to be affine, the following assumptions should be satisfied:

$$\bar{\mu}(X(t)) = a_0 + a_1 X(t)$$

$$\bar{\sigma}(X(t))\bar{\sigma}(X(t))^T = (c_0)_{ij} + (c_1)_{ij}^T X(t)$$

$$r(X(t)) = r_0 + r_1^T X(t)$$

This means that the drift, volatility, and interest rates should depend only linearly with respect to the state variable. Duffie et al. (2000) show that when you have an affine diffusion process, the discounted characteristic function is defined as follows:

$$\phi(X(t), t, T, u) = E^Q \left[ e^{-\int_t^T r(X_s) ds} e^{iuX_T} \mid F(t) \right] \quad (\text{A.2})$$

with boundary condition being:

$$\phi(X(t), T, T, u) = e^{iu^T X_T} \quad (\text{A.3})$$

has a solution:

$$\phi(X(t), t, T, u) = e^{A(u,t,T) + B(u,t,T)^T X(t)} \quad (\text{A.4})$$

$A(u, t, T)$  and  $B(u, t, T)^T$  are found when we solve the PDE of the process at hand. We will use the Black scholes as a demonstration but before we proceed we should mention that after solving the PDE we get  $A(u, t, T)$  and  $B(u, t, T)^T$  by the following Ricatti ODEs:

$$\frac{d}{d\tau} A(u, \tau) = -r_0 + B^T a_0 + \frac{1}{2} B^T c_0 B \quad (\text{A.5})$$

$$\frac{d}{d\tau} B(u, \tau) = -r_1 + a_1^T B + \frac{1}{2} B^T c_1 B \quad (\text{A.6})$$

### A.1.1 Example using Black Scholes

Dutillo et al. (2021) present the following example on finding A&B and testing for affinity. The stock price has the following process under Black-Scholes:

$$d(S(t)) = rS(t)dt + \sigma S(t)dW^Q(t) \quad (\text{A.7})$$

Testing the second condition mentioned above to check if the process is affine:

$$\bar{\sigma}(S(t))\bar{\sigma}(S(t)) = \sigma^2 S(t)^2 \quad (\text{A.8})$$

This process is clearly not affine as volatility is not linearly related to the stock price process. Hence, we consider the log-normal of  $S(t)$  which is affine as presented below. The SDE of  $x(t) = \log S(t)$  is :

$$d \log S(t) = (r - \frac{1}{2}\sigma^2)dt + \sigma dW^Q(t) \quad (\text{A.9})$$

Testing for affinity:

$$\bar{\mu}(X(t)) = r - \sigma^2 + 0x(t)$$

$$\bar{\sigma}(X(t))\bar{\sigma}(X(t))^T = \sigma^2 + 0x(t)$$

$$r(X(t)) = r + 0x(t)$$

where  $a_1$ ,  $c_1$ , and  $r_1$  are all zeros. We also have by substitution,  $a_0 = r - \frac{1}{2}\sigma^2$ , and  $c_0 = \sigma^2$ . Drift, interest rate, and volatility are all linearly dependent on the state variable making the log of  $S(t)$  affine. Setting up the system of ODEs to get  $A(u,\tau)$  and  $B(u,\tau)$ :

$$\frac{d}{d\tau}A(u, \tau) = -r_0 + B(u, \tau)a_0 + \frac{1}{2}B(u, \tau)c_0B(u, \tau) \quad (\text{A.10})$$

$$\frac{d}{d\tau}B(u, \tau) = -r_1 + a_1B(u, \tau) + \frac{1}{2}B(u, \tau)c_1B(u, \tau) \quad (\text{A.11})$$

By substituting the values above we get:

$$\frac{\partial}{\partial\tau}B(u, \tau) = 0$$

$$\frac{\partial}{\partial\tau}A(u, \tau) = -r + \left(r - \frac{1}{2}\sigma^2B(u, \tau)\right) + \frac{1}{2}\sigma^2B(u, \tau)B(u, \tau)$$

with boundary conditions:

$$B(u, 0) = iu$$

$$A(u, 0) = 0$$

We then finally obtain our two values for A&B:

$$B(u, \tau) = iu \quad (\text{A.12})$$

$$A(u, \tau) = \left[-r + iu\left(r - \frac{1}{2}\sigma^2 - \frac{1}{2}u^2\sigma^2\right)\right] \tau \quad (\text{A.13})$$

Using equation A.4, The characteristic function for the Black-Scholes model is defined as:

$$\phi(u, \tau) = e^{A(u, \tau) + B(u, \tau)x_0} \quad (\text{A.14})$$

By directly substituting,

$$\phi(u, \tau) = e^{iu \log S_0 + iu\left(r - \frac{1}{2}\sigma^2\right)\tau - \frac{1}{2}u^2\sigma^2\tau - r\tau} \quad (\text{A.15})$$

The same idea can be expanded to find the characteristic function for Bates and other stochastic volatility models who are affine.

## A.2 Stochastic Volatility Models

### A.2.1 Cox-Ingersoll-Ross

One of the advantages of the model compared to other models that model volatility is that the equation forces volatility to be non-negative.

$$dV_t = \kappa(\theta - V_t)dt + \sigma\sqrt{V_t}dW_t \quad (\text{A.16})$$

CIR model is usually used to model variables who exhibit a mean reversion phenomena such as interest rates and volatility. CIR processes could be modelled using the chi-square distribution or the closed form solution. It is worth mentioning that to avoid volatility to hit zero, the Feller condition is imposed,  $2\kappa\theta > \sigma^2$ . If the condition is not satisfied, there will be an accumulation of probability mass around zero making the left tail grow rapidly and unrealistically.

### A.2.2 Heston Model

To negate one of the main assumptions in the Black Scholes model regarding constant volatility, Heston (1993) add a new dimension to the BS model by assuming stochastic volatility.

$$dS_t = (r - q - \lambda\mu_J)S_t dt + \sqrt{V_t}S_t dW_t \quad (\text{A.17})$$

$$dV_t = \kappa(\theta - V_t)dt + \sigma\sqrt{V_t}dZ_t \quad (\text{A.18})$$

where the two Brownian motions have a correlation  $\rho dt$ . We can see that Bates is simply a Heston model with the jump component extension. The following is the

characteristic function of Heston if one wishes to model Heston using the characteristic function.

$$\phi = e^{A+B+C} \tag{A.19}$$

$$A = i\omega \log S_0 + i\omega(r - q)\tau$$

$$B = \frac{\theta\kappa}{\sigma^2}(\kappa - \rho\omega - d)\tau - 2\log\left(\frac{1 - ge^{-d\tau}}{1 - g}\right)$$

$$C = \frac{v_0}{\sigma^2} \left( \frac{(\kappa - \rho\omega - d)(1 - e^{-d\tau})}{1 - ge^{-d\tau}} \right)$$

$$d = \sqrt{\rho\sigma i\omega^2 + \sigma^2(i\omega + \omega^2)}$$

$$g = \frac{\kappa - \rho\omega - d}{\kappa - \rho\omega + d}$$

One can directly notice that the characteristic of Bates is the same as Heston but with the addition of  $D = -\lambda\mu_j i\omega\tau + \lambda\tau \left( (1 + \mu_j)^{i\omega} e^{\frac{1}{2}v_j i\omega(i\omega-1)} - 1 \right)$ . D is just adding the jump component on the CF of Heston, similar to what has been done when moving from Heston to Bates using the stock processes of the two equations.

## A.3 Varying the Parameters

Oosterlee and Grzelak (2019) clearly show the effect of the parameters on the volatility smile. He varies the values of the parameters and presents different smile curves for every parameter. A sample is shown below.

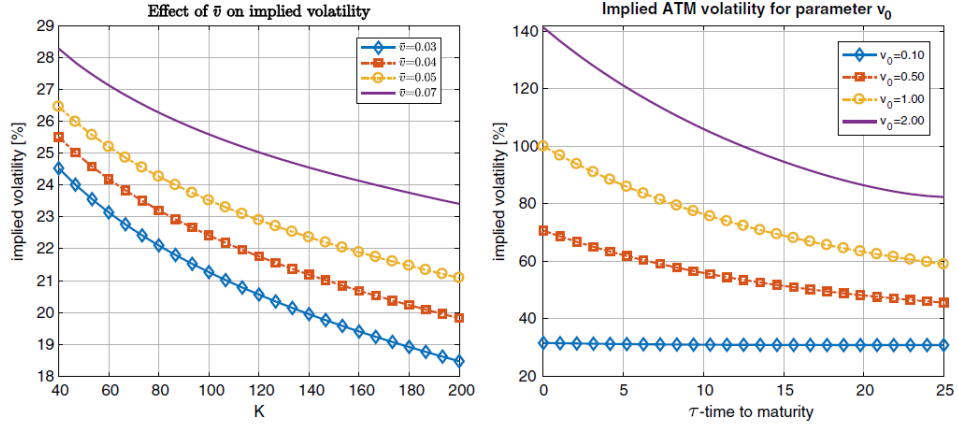


Figure A.1: Impact of varying  $v_0$  and  $\theta$

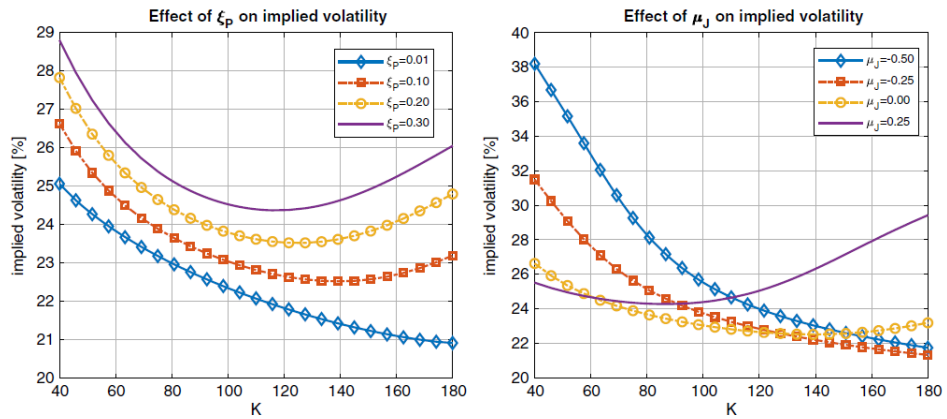


Figure A.2: Varying the jump parameters

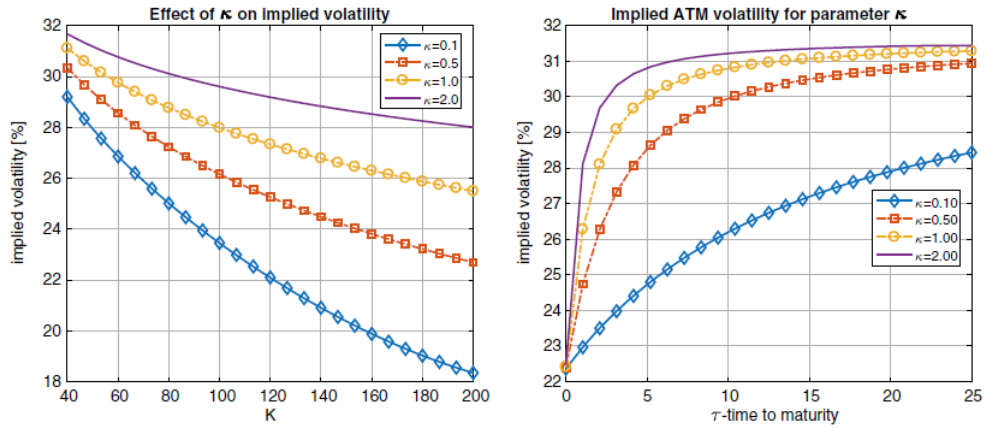


Figure A.3: Varying  $\kappa$

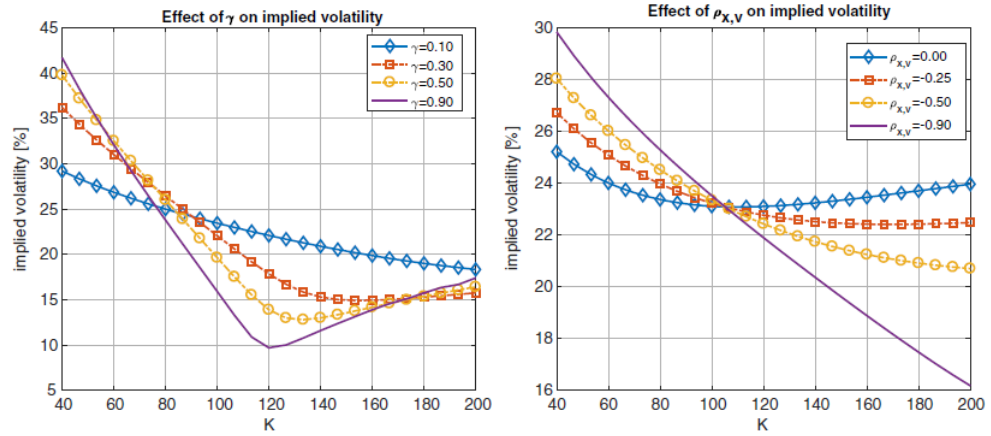
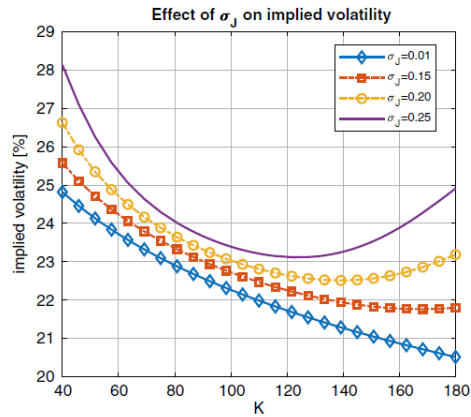


Figure A.4: Varying vol of vol and  $\rho$

Figure A.5: Varying  $\sigma_J$



The first thing to be noticed that the jump parameters provides higher implied

volatilities, and this is exactly why many academics and professionals would prefer Bates over Heston. Bates provide steeper skew on both tails of the smile which can be needed in times such as the pandemic. Oosterlee and Grzelak (2019) argue that the jump component increases the realized stock variance which increases the price of the option as the probability of ending up in the money increases.

## A.4 Nelder-Mead Algorithm

The Nelder-Mead method is a numerical technique that is used to find the maximum or minimum of a given function. The method does not use derivatives such as the gradient method usually used for finding implied volatility. A direct method is used where it calculates the value of the function and compares it to other values. The function minimized in our case is the objective function which we described earlier in the Data section. The algorithm uses a simplex, which is a shape that has one more vertex than the number of dimensions in the space. In our case, we have 9 vertices for our 8 parameters. The algorithm has six basic steps, starting with sorting . The illustration is adopted from Miles Chen’s lecture at UCLA. Suppose you want to evaluate the function at three points of the simplex,  $u$ ,  $v$  and  $w$ . The simplex in this case looks like a triangle If  $f(u) < f(v) < f(w)$  then  $u$  is the best performing point and  $w$  is the worst. From the worst point, we do a reflection that looks as follows:

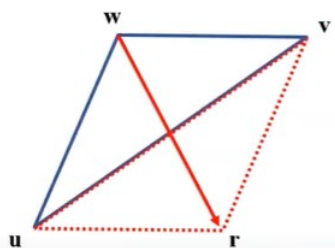


Figure A.6: Reflection Step

Now the new point  $r$  is evaluated against  $v$  and  $u$ . If the reflected point is the best out of three, we enter into the expansion step and we extend the point even

further. If not, we go into 'contraction' mode and contract along the line of the reflection. Two points are evaluated on that line, one is inside the contracted line and is quarter of the way between  $w$  and  $r$ . The other is on the outside and is three-quarter the line between  $w$  and  $r$ . If one of them is better than  $u$  and  $v$ , we go back to expansion mode. Otherwise, we 'shrink' and go back to step 1. The algorithm checks for convergence using the sample standard deviation of the simplex. If the standard deviation shrinks below a certain threshold  $\epsilon$ , we then have reached the proposed optimum. The same concept can be expanded to 3 or more vertices. Gao and Han (2012) talk about how inefficient the Nelder-mead algorithm becomes when the number of parameters becomes too high, which happens to be what Bates have. He proposes an alteration in the contraction, expansion and shrink steps to better suit the dimensions of the problem. His paper proves that his method works for high dimension optimization and is better than the standard algorithm. The least square optimization method using Nelder-mead is implemented in Python as `minimize(method='Nelder - Mead', adaptive=True)`. Adaptive is a boolean which takes True if one wants to use the updated algorithm by Gao and False if one prefers the standard method. Bounds are used throughout the minimization process, and we alter the boundaries once we see that the optimal parameter hits the boundary set by us.

To expand more on the steps that we explained mathematically, lets assume our objective function is  $f(x)$ , where  $x$  varies from 1 till  $N+1$ . Our simplex consists of  $N+1$  vertices.

**1) Ordering:** We order the vertices in order to satisfy  $f(x_1) \leq f(x_2) \leq f(x_3) \leq \dots \leq f(x_{n+1})$ .

**2) Calculate:** We calculate the centroid of the opposite of the worst vertex  $c = \frac{1}{n} \sum_{j \neq k} x_j$ , where  $x_h$  is the worst vertex.

**3) Reflection:** We reflect on the worst point and calculate it by

$$x_r = x_0 + \alpha(x_0 - x_n + 1) \quad (\text{A.20})$$

where  $\alpha > 0$ . If  $f(x_1) \leq f(x_r) \leq f(x_n)$ , we replace  $x_{n+1}$  with  $x_r$ . We then obtain a new simplex and we go back to step 1 until our condition is satisfied.

**4) Expansion:** if  $f(x_r) < f(x_1)$  which means that the reflection point is the best out of all the available vertices, we then compute the expanded point, which is an extension from the best available point,

$$x_e = x_0 + \gamma(x_r - x_0), \gamma > 1 \quad (\text{A.21})$$

After evaluating  $f(x_e)$  we compare it with the reflect point  $f(x_r)$ . If  $f(x_e) < f(x_r)$  then we replace  $x_{n+1}$  with the expansion point  $x_e$  and start back from Ordering. Otherwise, we replace the same worst point  $x_{n+1}$  with the reflection point  $x_r$  and go back to Ordering.

**5) Contraction:** Contraction consists of two steps. If  $f(x_n) \leq f(x_r) \leq f(x_{n+1})$ , we do what is known as 'Outside Contraction' and evaluate

$$x_{oc} = x_0 + \rho(x_r - x_0) \quad (\text{A.22})$$

where  $0 < \rho < 0.5$ . If  $x_{oc}$  is better than  $x_{n+1}$ , replace  $x_{n+1}$  with it, and go back to step 1. Otherwise, we move to step 6 which we will discuss below.

If  $f(x_r) > f(x_{n+1})$ , we compute  $x_{ic}$  which is 'inside contraction point'.

$$x_{ic} = x_0 + \rho(x_{n+1} - x_0) \quad (\text{A.23})$$

We then evaluate the function at that point and compare it with  $f(x_{n+1})$ . The same procedure in the outside contraction is adopted here.

**6) Shrink:** This is the step we referred to above and it says, for  $2 \leq i \leq n + 1$

$$x_i = x_1 + \sigma(x_i - x_1) \tag{A.24}$$

As for the values common used for the greeks in Nelder-Mead,  $\alpha = 1, \sigma = 0.5, \rho = 0.5, \gamma = 2$ . If one needs to have a faster calibration than the normal algorithm does, the shrink method can be ignored since many numerical studies have shown that shrink almost never occur when applying the algorithm. Singer and Singer (2004) elaborate more on efficient ways to implement this algorithm.